ACS APPLIED MATERIALS & INTERFACES

RESEARCH ARTICLE

www.acsami.org

# New Silicon Architectures by Gold-Assisted Chemical Etching

Bechelany Mikhael,*[,†,‡] Berodier Elise,[†] Maeder Xavier,[†] Schmitt Sebastian,[†] Michler Johann,[†] and Philippe Laetitia[†]

[†]EMPA, Swiss Federal Laboratories for Materials Science and Technology, Mechanics of Micro-Materials and Nanostructures, Feuerwerkerstrasse 39, CH-3602 Thun (Switzerland)

[‡]Institut Européen des Membranes (ENSCM UMR CNRS 5635), Université Montpellier 2, Place Eugène Bataillon, 34095 Montpellier, France

Supporting Information

**ABSTRACT:** Silicon nanowires (SiNWs) were produced by nanosphere lithography and metal assisted chemical etching. The combination of these methods allows the morphology and organization control of Si NWs on a large area. From the investigation of major parameters affecting the etching such as doping type, doping concentration of the substrate, we demonstrate the formation of new Si architectures consisting of organized Si NW arrays formed on a micro/mesoporous silicon layer with different thickness. These investigations will allow us to better understand the mechanism of Si etching to enable a wide range of applications such as molecular sensing, and for thermoelectric and photovoltaic devices.

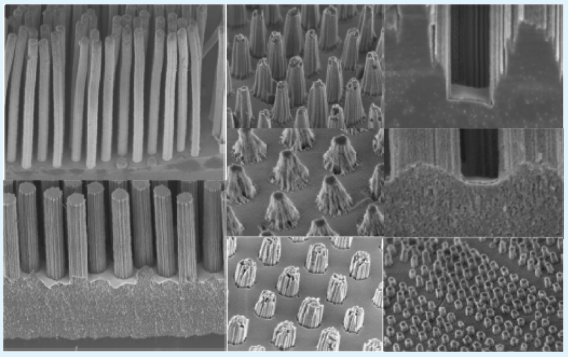

**KEYWORDS:** silicon nanowires, nanosphere lithography, metal-assisted chemical etching, gold, etching mechanism, EDX mapping

## INTRODUCTION

Silicon nanowires (Si NWs) have been the focus of intensive research over the past decade due to their unique electrical, mechanical and thermal properties. These NWs have been broadly explored in different fields such as field-effect transistors (FETs),[1] flexible large area electronics,[2] thermoelectric,[3] photovoltaics,[4−6] battery electrodes,[7] and electronic biosensors.[8] To date, different methods have been used to produce Si NWs such as chemical vapor deposition using the VLS (Vapor−Liquid−Solid) mechanism,[9] laser ablation,[10] thermal evaporation decomposition,[11] supercritical fluid liquid solid synthesis,[12] molecular beam epitaxy,[13] chemical etching,[14] and solution growth.[15] Among these methods, metal-assisted wet chemical etching of Si substrates is a promising method in combination with nanosphere lithography (NSL) to synthesize large areas of ordered Si NWs.

Fabrication of porous Si by metal assisted chemical etching was first proposed by Li and Bohn in 2000.[16] According to their report, a porous Si layer can be formed easily and efficiently by immersing Si wafers coated with a noble metal thin film in HF/$H_2O_2$ solution. Later the influence of shape of the deposit and of the metal species (Ag, Au, Pt, Au−Pd) were investigated by Asoh[17] and identified as special parameters that affect the morphology of the etched Si surface. In addition, Zhang[18] and co-workers have identified other factors affecting the morphology of Si NWs arrays such as the doping type and concentration, crystallographic orientation of the starting Si wafer, and the concentration of $H_2O_2$ in a chemical etching process. Meanwhile, Chatrier et al.[19] have shown that the etching solution composition is an important parameter for the surface morphology. The pioneering studies of Si etching identified the mechanism of Si etching as a localized electrochemical process. It is suggested that at the noble metal surface a cathodic reaction takes place reducing the oxidizing agent from the etching solution.[20] At Si surface an anodic reaction occurs, the Si is dissolved into an aqueous complex. Different metal etching mechanisms were suggested. Chen et al.[21] identified a link between temperature and crystallographic orientation of Si NWs, whereas in the work of Huang the oxidation rate affects Si NW orientation.[22] To produce highly ordered Si nanowires, Huang et al.[23] developed a simple method based on nanosphere lithography, enabling control of the diameter, the length, as well as the density of nanowire arrays. This approach allows the control of the doping type, doping concentration, crystallographic orientation, and the orientation of Si NWs relative to the Si substrate. On the basis of this method, several approaches[24−30] have been developed to fabricate Si NW arrays with various diameters, Si NWs with sub-10 nm diameter, vertically aligned non-(100) Si NW arrays relative to the substrate, as well as SiGe superlattice NW arrays. Recently, Chiappini et al.[31] shows the morphology tuning of nonorganized Si NWs (solid nanowires, porous nanowires, porous nanowires on porous layers, porous silicon layers or polished surfaces) by controlling a few key etching parameters (silicon resistivity, $H_2O_2$ concentration, ethanol concentration).

In this paper, the formation of new Si architectures consisting of organized Si NW arrays formed on a Si (micro/meso) porous

Received: May 31, 2011
Accepted: September 1, 2011
Published: September 01, 2011

  

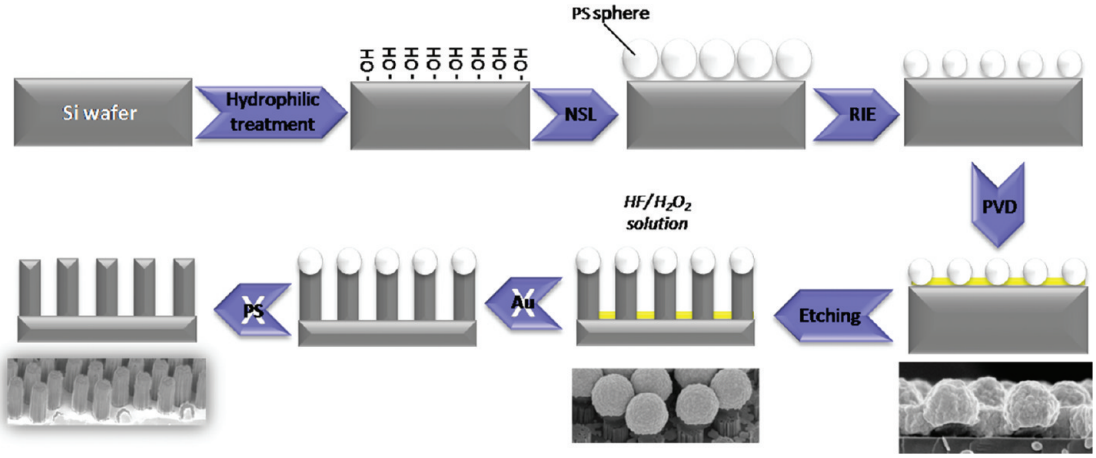


**Figure 1.** Schematic diagram showing the overall process to produce Si NW arrays by Au chemical etching combined with nanosphere lithography.

layer with different thickness is reported. We use a Au antidot array produced by NSL to produce Si NW arrays by a chemical etching method. The systematic investigation of the properties of Si (doping type and concentration) and the oxidant concentration as well as the Au repartition by EDX mapping during the etching of organized areas of Si NWs reveal the mechanism of the formation of these architectures. The ability to control the shape (circular or conic) and the porosity (dense or highly porous) of organized Si NWs opens opportunities to improve the properties of Si NWs for application in different fields such as solar cells, sensors, electronics,[32,33] thermoelectrics as well as fundamental studies on their physical properties.[34]

## MATERIALS AND METHODS

**Formation of Organized Si Nanowires.** Commercially available PS microsphere suspension ($d \approx 900$ nm, 2.53 wt % aqueous dispersion) was used (Polysciences, Inc., Eppelheim, Germany) as received. Acetone, toluene, HF (48%), $H_2SO_4$ (98%), sodium dodecyl sulfate solution, and $H_2O_2$ (30%), were purchased from Aldrich. n-type Si wafers (>10 and 0.002 Ω cm) and p-type Si wafers (>10 and 0.002 Ω cm), (100) crystal orientation, from Silicon Materials were used as substrates and are indexed respectively in this paper as n, $n^+$, p, and $p^+$. In a standard procedure, Si wafers were cut into 1.5 $cm^2$ pieces and precleaned in acetone for 5 min and in 1 wt % HF for 5 min to remove both organic contaminants and the native oxide. Additionally, the specimens were immersed in $H_2O_2/H_2SO_4$ solution for 10 min and afterward treated by $O_2$ plasma to produce a hydrophilic surface. After this pretreatment, a monodisperse suspension of 10 μL of polystyrene (PS) microspheres was released onto the substrate. Then the sample was immersed into deionized water. Two droplets of sodium dodecyl sulfate solution (10%) were deposited onto the water surface and the sample was removed out of the water, holding it tilted in order to remove PS spheres in excess to the PS monolayer. The sample was dried in air at room temperature and spheres self-assembled into a close-packed, two-dimensional ordered lattice via attractive capillary forces. After the complete evaporation of the solvent, the spheres were reduced for 1 min by reactive ion etching process (RIE) in order to obtain a nonclose packed array of spheres. In order to stick the PS spheres at the Si surface, a heat treatment at 100 °C for 30 min was performed. Then a thin Au film was deposited by sputtering. The sputtering was carried out at a discharge of 25 mA in a vacuum with a pressure below 0.1 mbar. By this physical vapor deposition (PVD) step a mask of Au was obtained and the thickness of this layer was measured around 400 nm (see Figure S1 in the Supporting Information) between the spheres. The specimen covered by Au were etched in a solution of $HF/H_2O_2$ in water at room temperature. Different etching solutions were used, with 4 M of HF and varying $H_2O_2$ concentration from 0.1 to 2M. After removing the metal with aqua regia solution and immersing the sample into toluene at 50 °C to dissolve the PS spheres, Si samples were dried and fully characterized. Figure 1 shows the overall process to produce Si NW arrays.

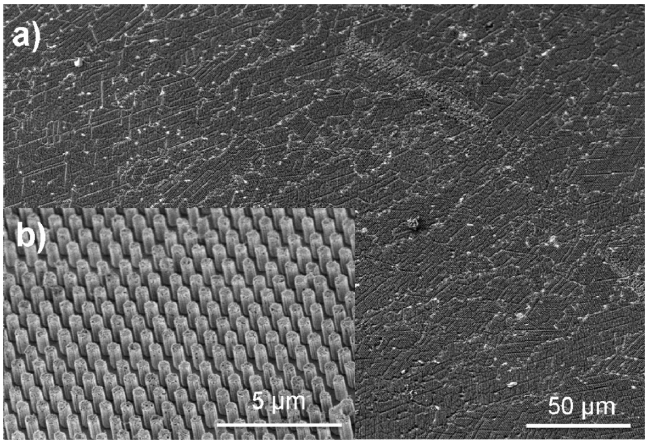


**Figure 2.** (a, b) SEM images at different magnifications of a regular pattern of p-type Si NWs with 1 μm periodicity etched in $HF/H_2O_2$ (4 M/0.88 M) for 1 min.

**Characterization.** Ordered geometric patterns are characterized by scanning electron microscopy (SEM, Hitachi S-4800), and energy-dispersive X-ray spectroscopy (EDX, Genesis 4000 EDAX).

## RESULTS AND DISCUSSION

**Production of Si NWs.** The fabrication process employed in the formation of Si NWs is illustrated in Figure 1. In a standard procedure, a p-type Si wafer (>10 Ω cm; indexed p) was etched in a water solution of $HF/H_2O_2$ (4 M/0.88 M) at room temperature for 1 min. After removal of the metal and the PS spheres, specimens were dried and fully characterized. Figure 2a shows the regular pattern of Si NWs synthesized by metal assisted etching. The Si NWs, with long-range hexagonal ordering, have a diameter of 400 nm and a length of about 1 μm

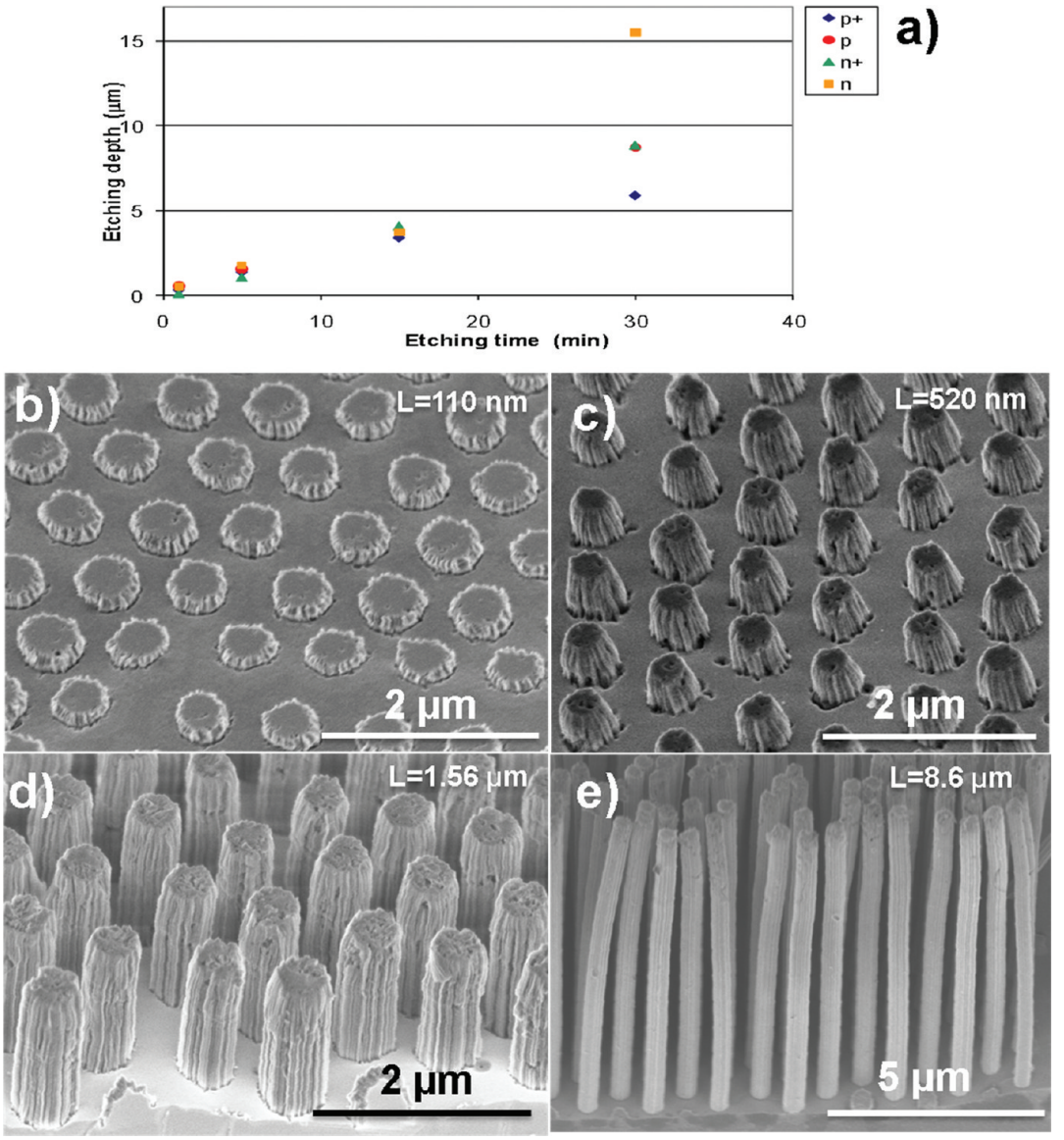


**Figure 3.** (a) Etching depth as a function of the etching time duration for 4 kinds of Si substrate $p^+$, p, $n^+$, and n. The Si NWs with 1 $\mu$m periodicity were etched in $HF/H_2O_2$ (4 M/0.88 M) solution. Every point is the average of 4 measurements. (b−d) As an example, SEM images (cross-section tilted view 50°) of a regular pattern of p-type Si NWs with 1 $\mu$m periodicity etched in $HF/H_2O_2$ (4 M/0.88M) for (b) 15 s, (c) 30 s, (d) 1 min, and (e) 30 min.

(Figure 2b). Au was deposited by sputtering onto the Si substrate covered with the nonclose-packed PS sphere mask. This process resulted in a Au antidot arrays consisting of a continuous layer of Au NPs (see Figure S1 in the Supporting Information).[35,36] The diameter of the pores was determined by the diameter of the PS spheres after RIE, basically this area corresponds to the contact surface between the PS spheres and the Si substrate.[35] EDX spectrum shows that Si and O are the main detected elements. Thus, no Au remained after the cleaning process.

**Influence of Time.** To study the influence of etching time on the morphology of the obtained NWs, we dipped patterned p and n-type Si wafers with different doping concentration in the $HF/H_2O_2$ (4 M/0.88 M) for 1, 5, 15, and 30 min (Figure 3a). These specimens are indexed p (low boron doped: >10 Ω cm), $p^+$ (high boron doped: 0.002 Ω cm), n (low phosphorus doped: >10 Ω cm) and $n^+$ (high phosphorus doped: 0.002 Ω cm) in the manuscript. The etching depths were measured by SEM and plotted in the Figure 3a. It shows that the length of Si NWs is proportional to the immersion time of the Si samples into the etching solution. As an example, Figure 3b−e shows SEM images of a regular pattern of p-type Si NWs with 1 $\mu$m periodicity etched in $HF/H_2O_2$ (4 M/0.88 M) for 15 s, 30 s, 1 min,and 30 min, respectively. Their lengths varied from 110 nm to about 9 $\mu$m.

**Influence of $H_2O_2$ Concentration.** Figure 4b shows a SEM image of a regular pattern of p-type Si NWs with 1 $\mu$m periodicity etched in $HF/H_2O_2$ (4 M/0.88M) for 5 min. The length of Si NWs is approximately 4 $\mu$m and they are etched straight (perpendicular to the surface of Si sample) and uniform (dimension and shape) on the whole Si wafer. Figure 4d shows Si NWs produced with a lower concentration of oxidant $HF/H_2O_2$ (4 M/0.1M) for the same processing time. The Si NWs produced are smaller; the length is about 800 nm. The diameter and the morphology remained unchanged by changed $H_2O_2$ concentration. We noted that porosity has been found in

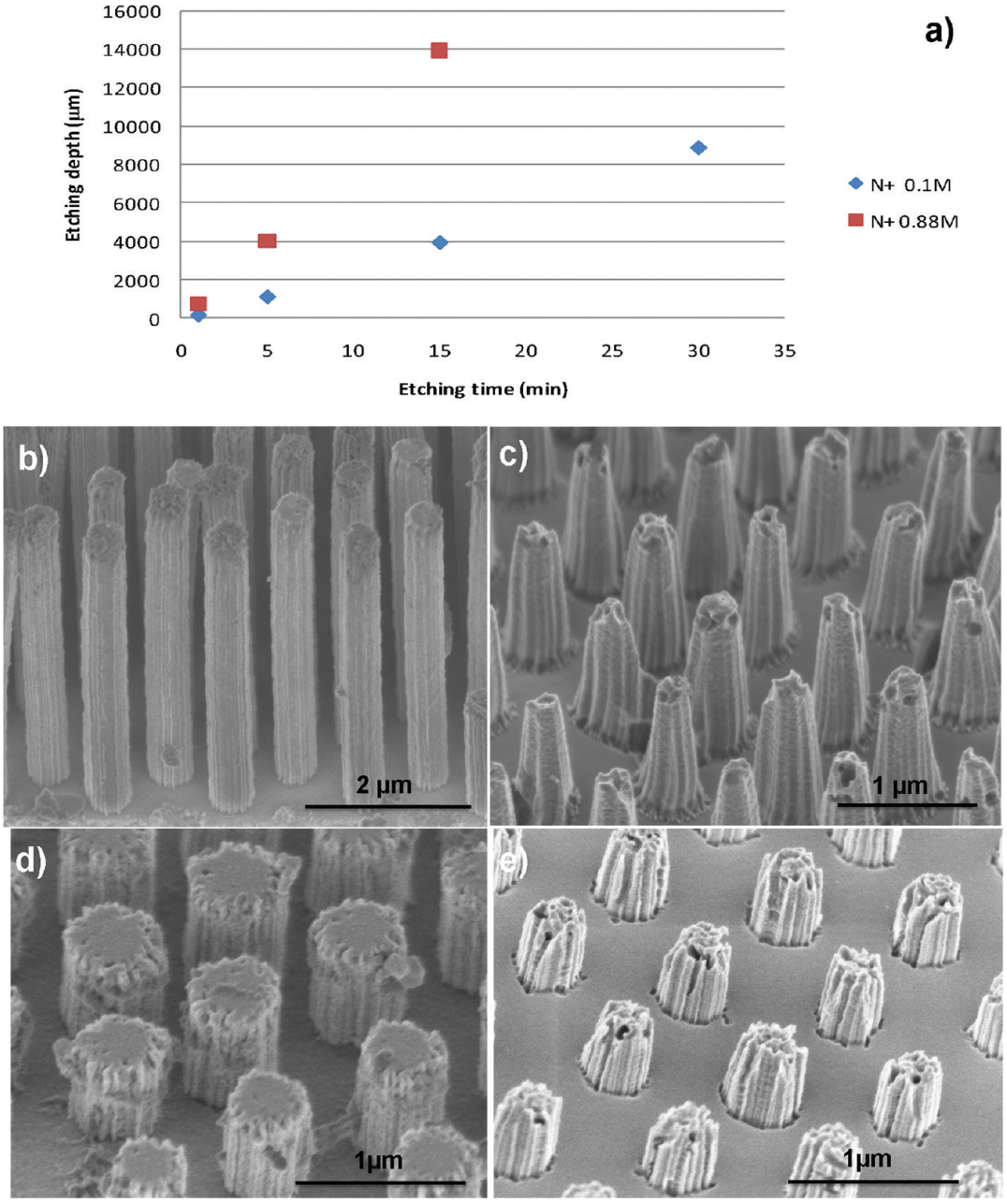


**Figure 4.** (a) Etching depth as the function of the etching time for 2 solutions of $HF/H_2O_2$ (4 M/*x* M): high $H_2O_2$ concentration (0.88M) and low $H_2O_2$ concentration (0.1 M). The $n^+$ doped Si NWs are with 1 $\mu$m periodicity. Every point is the average of 4 measurements. SEM images (cross-section tilted view 50°) of a regular pattern of p-type Si NWs with 1 $\mu$m periodicity etched for 5 min into: (b) $HF/H_2O_2$ (4 M/0.88 M) and (d) $HF/H_2O_2$ (4 M/0.1M) solution. (c, e) SEM images of the Si NWs in b and d, respectively, after immersion in HF 1% for 3 min.

connection with metal-assisted etching.[19,20,31] By immersing the samples into a 1% HF solution for 3 min, we removed the native oxide and the porous silicon. Images c and e in Figure 4 show the SEM images of the Si NWs after immersion from images b and d, respectively, Figure 4. The final Si NWs exhibited a slightly conic shape. Furthermore, the initial length of the Si NWs from Figure 4b ($L$ = 4 $\mu$m) was longer than those from Figure 4d ($L$ = 1 $\mu$m). The amount of Si removed has been found higher for the Si NWs from Figure 4b ($L$ = 1, 5 $\mu$m in Figure 4c), i.e., etched with the higher oxidant concentration than in Figure 4d ($L \approx 1$ $\mu$m in Figure 4c). Therefore, the increasing of the $H_2O_2$ concentration involves a larger porous layer on the SiNWs walls and a conic shape. The formation of these conic nanostructures will be discussed in details in the mechanism part.

**Influence of Doping.** Figure 5 shows the SEM images of Si NWs etched in $HF/H_2O_2$ (4 M/0.1) for 5 min with different doping concentrations and types. Images a and b in Figure 5 illustrate the morphologies of Si NWs with high doping concentration, $p^+$-doped and $n^+$-doped, respectively. Images c and d in Figure 5 illustrate the morphology of Si NWs with low doping concentration: p-doped and n-doped, respectively. Related to low doped substrates, the depth difference rises. From SEM pictures, we measured 1.65 $\mu$m of length with a p-doped substrate and from the n-doped substrates about 1.85 $\mu$m.

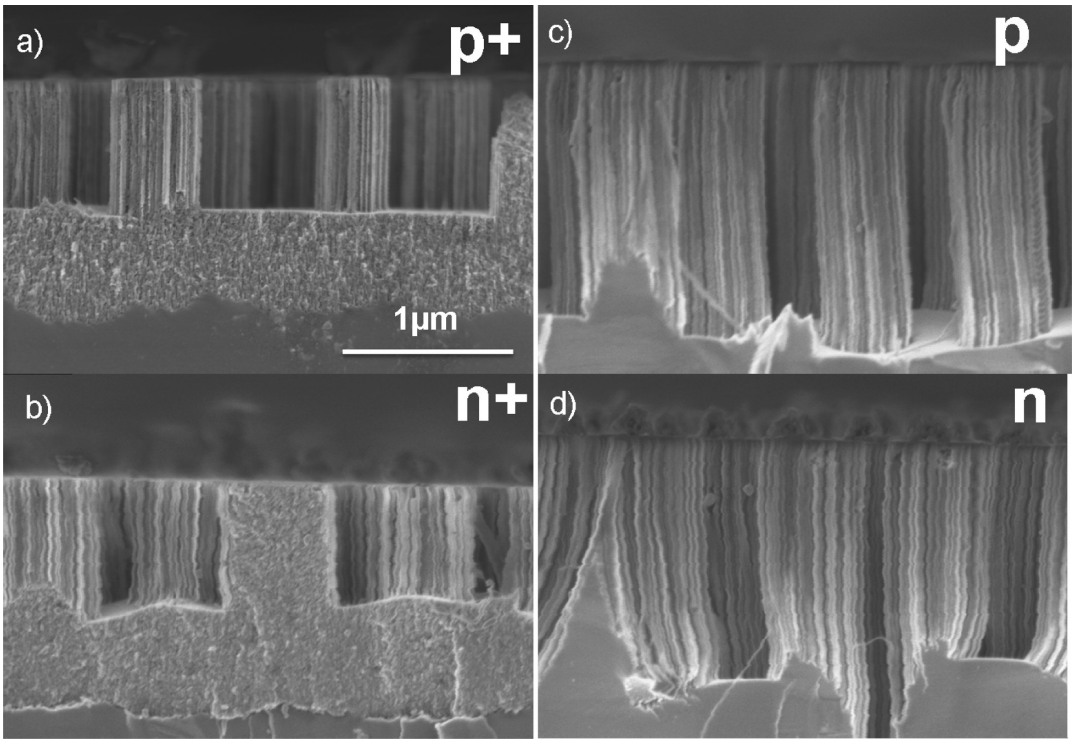


**Figure 5.** (a) SEM images (cross-section tilted view 50°) of a regular pattern of Si NWs with 1 $\mu$m periodicity etched in $HF/H_2O_2$ (4 M/0.1 M) for 5 min with different doping concentration and type: (a) $p^+$, (b) $n^+$, (c) p, and (d) n-type Si substrates.

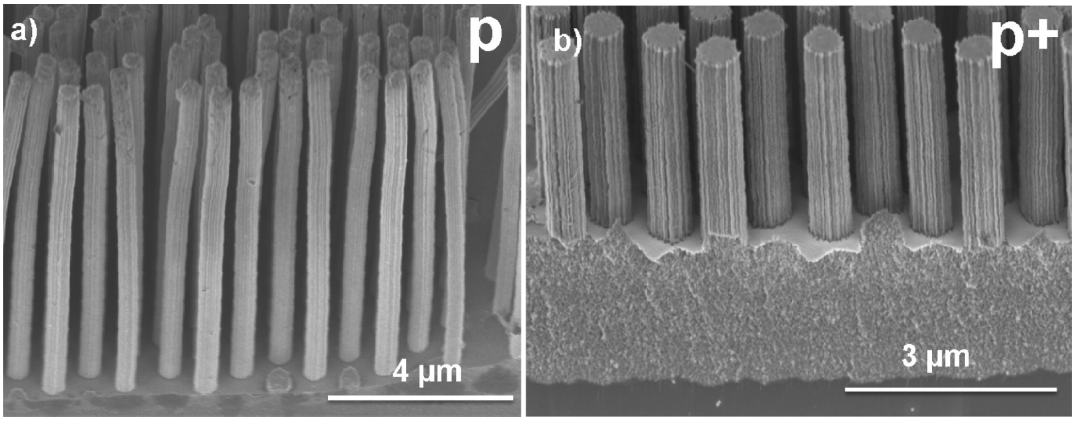


**Figure 6.** (a) SEM images (cross-section tilted view 50°) of a regular pattern of Si NWs with 1 $\mu$m periodicity etched in $HF/H_2O_2$ (4 M/0.1 M) for 30 min with different doping concentration and type: (a) p and (b) $p^+$-doped substrates.

Therefore, n-doped silicon is assumed to be etched faster than p-doped. Zhang et al.[18] have found the same tendency for a 7−13 Ω cm doping concentration and our further experiments for longer etching duration (Figure 3) confirmed this finding. Thus doping type (p- or n-doped) influences the etching rate of Si. Figures 5 and 3a show that for the same type of doping (n or p), the p substrate with the lower doping concentration showed deeper etching than $p^+$. That is in agreement with Megouda's work, who reported that the length of NWs increases by decreasing the resistivity.[37] The SEM images (Figure 5a,b) show the formation of porous Si NWs and porous layer underneath for both p and n-type high doped substrate. The values plotted in Figure 3a, include the porous layer in the measurement of the etching depth. To better illustrate this porosity we etched the samples during a longer time. On Figure 6a, Si NWs are regular, straight (perpendicular to the substrate) and without any porosity. On the higher doped Si substrate (Figure 6b) etched on the same conditions, we saw a bistructure formed of porous Si NWs on Si meso/microporous layers.

**Au EDX Mapping.** Many authors as for instance Migouda et al.[37] assimilated the presence of meso/microporosity during the etching process to gold particles. They suggested that Ostwald ripening mechanism would occur during the etching process. Au nanoparticles (NPs) would etch while they would sink into the bulk Si and would form porous silicon. Others as for instance Chiappini et al.[31] proposed hypothesizes that the porosification is catalyzed by the metal ions in solution without formation of secondary NPs. EDX mapping has been performed

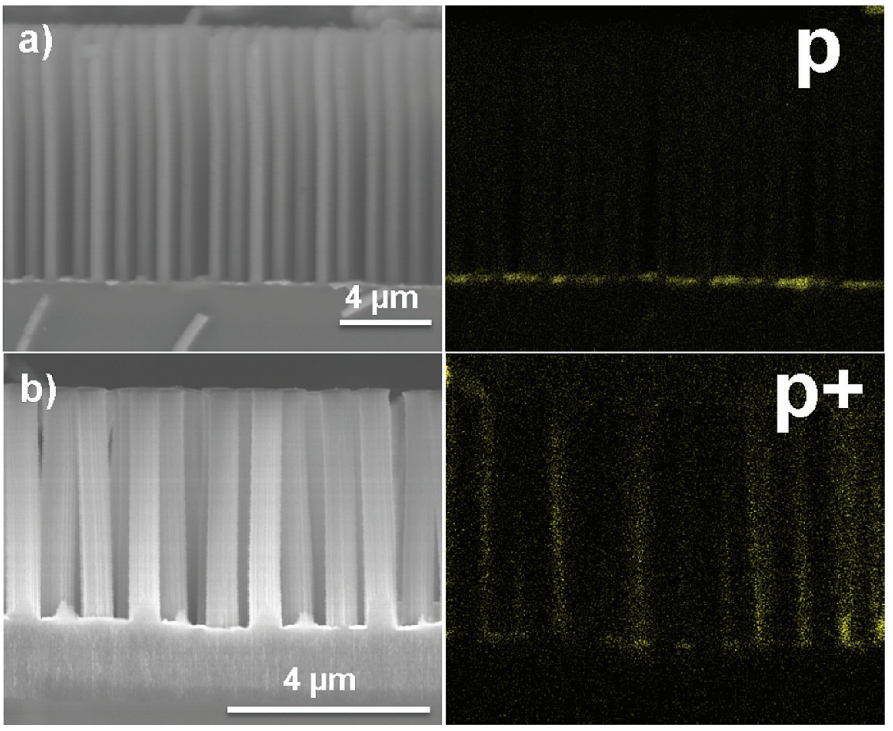


**Figure 7.** (a) EDX mapping of a regular pattern of Si NWs with 1 $\mu$m periodicity etched in $HF/H_2O_2$ (4 M/0.88 M) for 30 min in p-doped Si wafers and (b) EDX mapping of a regular pattern of Si NWs with 1 $\mu$m periodicity etched in $HF/H_2O_2$ (4 M/0.1 M) for 30 min in $p^+$-doped Si wafers; Au distribution is represented in yellow.

during SEM analysis (cross section) to evaluate the distribution of Au on the nanostructures. Because of the complex shape of the NSs, EDX measurements give qualitative information and do not allow quantitative measures. Figure 7a shows the EDX mapping (spot size 20−30 nm) recorded in parallel with SEM observations of a regular pattern of Si NWs with 1 $\mu$m periodicity etched in $HF/H_2O_2$ (4 M/0.88 M) for 30 min on p doped Si wafers. Figure 7b shows EDX mapping of a regular pattern of Si NWs with 1 $\mu$m periodicity etched in $HF/H_2O_2$ (4 M/0.1 M) for 30 min $p^+$ doped Si wafers. Au signal intensity is represented in yellow. On the low doped Si substrate (Figure 7a), Au was found only at the bottom of the hole created by the Au antidot arrays. Au was detected neither on the NWs walls nor into the silicon sample. Moreover, the variation of the oxidant concentration does not show any significant difference on the Au distribution (see Figure S3 in the Supporting Information). However, the mapping done on the high doped Si NWs (Figure 7b), localized Au not only at the bottom of the holes created by the Au antidot arrays etching but also along the side walls of the Si NWs. No Au NPs were found into the porous layer underneath the Si NWs. Again, no significant difference is observed when using different doping type and different oxidant concentration.

**Discussion on the Mechanism of Etching of These Si Architectures.** Basically, assisted chemical etching is based on electrochemical processes where a Si wafer covered by a metal layer is immersed in the HF and $H_2O_2$ solution. In our case, the Si substrate covered by spheres is in contact with a Au antidot arrays and etched in a solution composed of $HF/H_2O_2$. The first step of the reaction might be the reduction of the $H_2O_2$ at the metal/solution interface that can be called cathodic site. The reduction is like following:

$$H_2O_2 + 2H^+ + 2e^- \rightarrow 2H_2O$$

$e^-$ are taken from the gold that dissolved in ions following the dissolution reaction

$$Au \rightarrow Au^{3+} + 3e^-$$

Au is more electronegative than Si, so Au ions are able to recover into gold by catching electrons from Si bulk. That involves an injection of positives charge carriers, called holes. They are locally injected underneath the gold layer. On this weakness site, Si is oxidized into $SiO_2$ and the attack by HF occurs afterward, and the $SiO_2$ becomes an aqueous byproduct.

$$SiO_2 + 6HF \rightarrow 2H_2O + H_2SiF_6$$

The Au layer sinks into the tracks around the PS and the Si NWs appear. We note here that RIE etching in an oxygen plasma atmosphere results in the formation of a thin oxide layers. The presence of this $SiO_2$ layer on the Au−Si interface will have a limited impact on the proposed etching model. When the Si wafer is immersed in the solution, HF dissolves the $SiO_2$ and the Au layer gets into contact with the Si surface.

**Influence of Oxidant.** The oxidant is considered as playing a major role in the etching process. Chartier et al.[19] studied the influence of the relative amount of HF and $H_2O_2$ on the etching rate and etched morphology. Their work revealed different regimes of dissolution depending of the etching solution composition. In our conditions $HF/H_2O_2$ (4 M/0.1 M) and $HF/H_2O_2$ (4 M/0.88 M) the HF concentration can be considered very high. Therefore, the etching rate is assumed to be completely determined by the $H_2O_2$ concentration and all the holes are supposed to be locally consumed. Images b and c in Figure 4 indicate that all the holes from the oxidant $H_2O_2$ were not consumed underneath the Au/Si interface but instead diffused along (resulting in the formation of porous layer on the top of

NWs). It was suggested that by increasing the oxidant concentration, more holes are injected into bulk Si and those not consumed locally escape and lead to a lateral transport of charge carriers in the surrounding area of the Au catalyst. Figure S4 in the Supporting Information well-emphasizes the holes diffusion around gold layer that involved micro/mesopores formation on the weakest sites (weakest crystallographic plane or defect) and confirms the Tsujino and Matsumura work[38] as well as Chapini et al. work.[31] Consequently, small pores are produced in the vicinity of the gold; they are these porous silicon areas that were removed during the second treatment into HF 1% for 3 min (Figure 4c). The conic shape would come from the longer exposure time of the top part according to Dawood et al.[39] Au mapping (Figure 7a) confirmed that this porosity comes from the lateral transport of charge carriers and not from gold redeposition/etching as reported elsewhere[40] because no gold has been detected in the top part of the side walls of the NWs.

**Influence of Doping.** Figures 5 and 3a revealed that doping type of Silicon influences its etching rate and that for the same type of doping (n or p), the substrate with the lower doping concentration presents deeper etching. The measurement showed also that the porosity of the NWs change with doping concentration (Figure 5). From these results we assume that the mechanism of etching is not the same for low and high doped Si.

For low doping concentration, n-doped silicon is assumed to be etched faster than p-doped. This is consistent as n-doped substrate is negatively doped, so more electrons would be available at the Au layer and reduce $H_2O_2$. The reduction would be facilitated which would involve a faster etching rate.

With high doping concentration, this assumption seems to fail. High n-doped substrates (i.e., high electrons concentration from impurities) exhibited smaller etched depth than Si low n-doped. This observation suggests a more complex etching mechanism related to high doped Si.

As observed in Figures 5 and 6, all the high doped substrates (p and n) presented an important layer of porosity on which Si NWs appeared. The repartition of Au by EDX mapping (Figure 7b in yellow) has shown no Au in the porous layer. Therefore, Au particles would not be responsible of the formation of the porosity. To emphasize this assumption we did a chemical etching combined with NSL without Au antidot arrays on a $p^+$-doped Si substrate. The SEM image (see Figure S5 in the Supporting Information) reveals the presence of a porous layer on the silicon surface similar to the porosity observed underneath the Si NWs in Figure 6b. We should not forget here that we have the formation of organized Si NWs without a porous layer on low doped Si (Figure 6a). Then, the bistructure produced with high doped Si substrates can be seen as a combination of Figure 6a and Figure S5 in the Supporting Information. That would mean Au-assisted chemical etching is in competition with chemical etching on the weak sites of the bulk high doped Si. The etched depth ratio between high and low doped Si substrates suggests that it is more a competition of progress than simultaneous processes. One would take places on the weakness sites, enhanced by the high concentration of carriers,[41] in other words where impurities are, and would produce isotropic porous layer. The other one would be assisted by the Au antidot arrays and would be the responsible of the Si NWs fabrication. Moreover EDX mapping showed the presence of Au on the sidewalls of Si NWs for high doped substrates at different $H_2O_2$ concentration (Figure 7b) and confirmed a third mechanism which would be involved in the etching process of Si NWs. Basically, one can assume that Au is dissolved from the Au antidot arrays and would than be redeposited on the sidewall of the Si NWs. These observations could explain why the high doped substrates exhibited smaller etched depth than Si low n-doped. Another explanation could be that the $HF/H_2O_2$ solution near the substrate is not only used for the metal assisted etching process but would be also involved in the isotropic etching of the porous layer.

Recently, Chiappini et al.[31] proposed hypothesizes that the SiNW formation is catalyzed by the primary NPs, whereas the porosification is catalyzed by the metal ions in solution without formation of secondary NPs. Our results do not support this model since our SEM image (see Figure S5 in the Supporting Information) reveals the presence of a porous layer on the silicon surface without the presence of metal ions in the etching solution.

**Charge Transfer Mechanism.** Charge transfer mechanism involves the hole injection process, which is well-documented for electroless etching of Si in $HF/HNO_3$ solution (stain etching).[19] The initiation of etching process can occur without any metal catalyst independently of the doping concentration. In short, any Si substrate (regardless doping type and concentration) will be etched in $HF/H_2O_2$. From a kinetic point of view, reduction of $H_2O_2$ or $O_2$ is more favorable onto the metal surface (acting as local cathode). As already described in the previous section, most of the phenomena in metal assisted etching are qualitatively explained by the charge transfer process from the metal to the Si substrate, such as the solution role in etching morphology, the doping concentration in the etched morphology, etc. Side reactions, such as hydrogen evolution, do not always influence the etching morphology, although diffusion of the hydrogen is suspected to play a role in the process. Since the charge transfer between metal and the Si substrate does occur, it is important to look at the electrochemical potential of different metals and Si band edges[17] and to keep in mind the surface band bending of Si for a reference metal. In other words, doping concentration and type, as well as Fermi level of metal or etchant in nature should all be discussed in the etching mechanism, which has not been done so far.

**Mass Transfer Diffusion.** Mass transfer diffusion of reactants and byproducts in the reaction should also control the morphology of the NWs. EDX could be used for looking at the gold motion during the process. At the interface of Au and Si, we can imagine side-products, and reactants. Reactants would only diffuse along this interface or through the noble metal. Both models have been already proposed in the literature and probably occur simultaneously, leading to more homogeneous etching at the metal/Si interfaces, on the side wall and the underneath Si.[42,43] Unfortunately, there is so far no possible evidence to distinguish which diffusion mechanism dominates.[20] We could imagine however, that side products (especially $H_2$ evolution) on the side walls. Thus, bubble evolution could either mechanically delaminates the metal surface from the Si substrate or partially prevent the etching, which would force the reactants to diffuse through the gold layer in another way.

## CONCLUSION

In summary, we used the NSL to produce Si NWs arrays by assisted chemical etching method. The systematic investigation on the properties of Si (doping type and doping concentration) and the oxidant concentration combined with EDX mapping provided pertinent information about the role of the substrate, etching solution and metal catalysis in the etching process. However, since none in situ method for observing the etching

process have been tempted here, the overall mechanism remains unclear. The investigation about etching mechanisms permitted to improve the production of organized arrays of Si NWs with controlled shape (circular or conic) and porosity (dense or highly porous). We demonstrated the formation of new Si architectures composed of organized Si NWs arrays formed on a Si porous (micro/meso) layer with different thickness. The understanding of etching mechanism has been improved especially related to the role of doping concentration of the Si substrate. The high control of major features of SiNWs suggests new applications in different fields such as solar cells, sensors, electronic, thermoelectronic as well as the fundamental study of their physical properties.

## ■ ASSOCIATED CONTENT

**Supporting Information.** Additional figures (PDF). This material is available free of charge via the Internet at http://pubs.acs.org/

## ■ AUTHOR INFORMATION

**Corresponding Author**

*Phone: +33 (0)4 67 14 91 67. Fax: +33 (0)4 67 14 91 19. E-mail: mikhael.bechelany@iemm.univ-lyon1.fr.

## ■ ACKNOWLEDGMENT

Financial support by the European Commission in the framework of the project Rod-sol (Contract 227497) is gratefully acknowledged. M.B. and E.B. contributed equally to this work.

## ■ REFERENCES

(1) Cui, Y.; Duan, X. F.; Hu, J. T.; Lieber, C. M. *J. Phys. Chem. B* **2000**, *104*, 5213–5216.
(2) McAlpine, M. C.; Friedman, R. S.; Jin, S.; Lin, K. H.; Wang, W. U.; Lieber, C. M. *Nano Lett.* **2003**, *3*, 1531–1535.
(3) Hochbaum, A. I.; Gargas, D.; Hwang, Y. J.; Yang, P. D. *Nano Lett.* **2009**, *9*, 3550–3554.
(4) Tian, B. Z.; Zheng, X. L.; Kempa, T. J.; Fang, Y.; Yu, N. F.; Yu, G. H.; Huang, J. L.; Lieber, C. M. *Nature* **2007**, *449*, 885–889.
(5) Garnett, E. C.; Yang, P. D. *J. Am. Chem. Soc.* **2008**, *130*, 9224–9225.
(6) Sivakov, V.; Andra, G.; Gawlik, A.; Berger, A.; Plentz, J.; Falk, F.; Christiansen, S. H. *Nano Lett.* **2009**, *9*, 1549–1554.
(7) Chan, C. K.; Peng, H. L.; Liu, G.; McIlwrath, K.; Zhang, X. F.; Huggins, R. A.; Cui, Y. *Nat. Nanotechnol.* **2008**, *3*, 31–35.
(8) Zheng, G. F.; Patolsky, F.; Cui, Y.; Wang, W. U.; Lieber, C. M. *Nat. Biotechnol.* **2005**, *23*, 1294–1301.
(9) Lerose, D.; Bechelany, M.; Philippe, L.; Michler, J.; Christiansen, S. *J. Cryst. Growth* **2010**, *312*, 2887–2891.
(10) Yang, Y. H.; Wu, S. J.; Chin, H. S.; Lin, P. I.; Chen, Y. T. *J. Phys. Chem. B* **2004**, *108*, 846–852.
(11) Pan, H.; Lim, S.; Poh, C.; Sun, H.; Wu, X.; Feng, Y.; Lin, J. *Nanotechnology* **2005**, *16*, 417–421.
(12) Yuan, F. W.; Tuan, H. Y. *Cryst. Growth Des.* **2010**, *10*, 4741–4745.
(13) Shao, M. W.; Ma, D. D. D.; Lee, S. T. *Eur. J. Inorg. Chem.* **2010**, 4264–4278.
(14) Zhang, Y. J.; Li, W.; Chen, K. J. *J. Alloy. Compd.* **2008**, *450*, 512–516.
(15) Chun, J. Y.; Lee, J. W. *Eur. J. Inorg. Chem.* **2010**, 4251–4263.
(16) Li, X.; Bohn, P. W. *Appl. Phys. Lett.* **2000**, *77*, 2572–2574.
(17) Asoh, H.; Arai, F.; Ono, S. *Electrochim. Acta* **2009**, *54*, 5142–5148.
(18) Zhang, M. L.; Peng, K. Q.; Fan, X.; Jie, J. S.; Zhang, R. Q.; Lee, S. T.; Wong, N. B. *J. Phys. Chem. C* **2008**, *112*, 4444–4450.
(19) Chartier, C.; Bastide, S.; Levy-Clement, C. *Electrochim. Acta* **2008**, *53*, 5509–5516.
(20) Huang, Z. P.; Geyer, N.; Werner, P.; de Boor, J.; Gosele, U. *Adv. Mater.* **2011**, *23*, 285–308.
(21) Chen, H. A.; Wang, H.; Zhang, X. H.; Lee, C. S.; Lee, S. T. *Nano Lett.* **2010**, *10*, 864–868.
(22) Huang, Z. P.; Shimizu, T.; Senz, S.; Zhang, Z.; Geyer, N.; Gosele, U. *J. Phys. Chem. C* **2010**, *114*, 10683–10690.
(23) Huang, Z. P.; Fang, H.; Zhu, J. *Adv. Mater.* **2007**, *19*, 744–748.
(24) Huang, Z. P.; Shimizu, T.; Senz, S.; Zhang, Z.; Zhang, X. X.; Lee, W.; Geyer, N.; Gosele, U. *Nano Lett.* **2009**, *9*, 2519–2525.
(25) Choi, W. K.; Liew, T. H.; Dawood, M. K. *Nano Lett.* **2008**, *8*, 3799–3802.
(26) Huang, Z. P.; Zhang, X. X.; Reiche, M.; Liu, L. F.; Lee, W.; Shimizu, T.; Senz, S.; Gosele, U. *Nano Lett.* **2008**, *8*, 3046–3051.
(27) Chang, S. W.; Chuang, V. P.; Boles, S. T.; Ross, C. A.; Thompson, C. V. *Adv. Funct. Mater.* **2009**, *19*, 2495–2500.
(28) Peng, K. Q.; Zhang, M. L.; Lu, A. J.; Wong, N. B.; Zhang, R. Q.; Lee, S. T. *Appl. Phys. Lett.* **2007**, *90*, 103117.
(29) Wang, X.; Pey, K. L.; Choi, W. K.; Ho, C. K. F.; Fitzgerald, E.; Antoniadis, D. *Electrochem. Solid St* **2009**, *12*, K37–K40.
(30) Geyer, N.; Huang, Z. P.; Fuhrmann, B.; Grimm, S.; Reiche, M.; Nguyen-Duc, T. K.; de Boor, J.; Leipner, H. S.; Werner, P.; Gosele, U. *Nano Lett.* **2009**, *9*, 3106–3110.
(31) Chiappini, C.; Liu, X. W.; Fakhoury, J. R.; Ferrari, M. *Adv. Funct. Mater.* **2010**, *20*, 2231–2239.
(32) Dejeu, J.; Bechelany, M.; Philippe, L.; Rougeot, P.; Michler, J.; Gauthier, M. *ACS Appl. Mater. Interfaces* **2010**, *2*, 1630–1636.
(33) Dejeu, J.; Bechelany, M.; Rougeot, P.; Philippe, L.; Gauthier, M. *ACS Nano* **2011**, *5*, 4648–4657.
(34) Mook, W. M.; Niederberger, C.; Bechelany, M.; Philippe, L.; Michler, J. *Nanotechnology* **2010**, *21*, 055701/1–055701/9.
(35) Bechelany, M.; Maeder, X.; Riesterer, J.; Hankache, J.; Lerose, D.; Christiansen, S.; Michler, J.; Philippe, L. *Cryst. Growth Des.* **2010**, *10*, 587–596.
(36) Bechelany, M.; Brodard, P.; Elias, J.; Brioude, A.; Michler, J.; Philippe, L. *Langmuir* **2010**, *26*, 14364–14371.
(37) Megouda, N.; Hadjersi, T.; Piret, G.; Boukherroub, R.; Elkechai, O. *Appl. Surf. Sci.* **2009**, *255*, 6210–6216.
(38) Tsujino, K.; Matsumura, M. *Electrochim. Acta* **2007**, *53*, 28–34.
(39) Dawood, M. K.; Liew, T. H.; Lianto, P.; Hong, M. H.; Tripathy, S.; Thong, J. T. L.; Choi, W. K. *Nanotechnology* **2010**, *21*, 205305.
(40) Qu, Y. Q.; Liao, L.; Li, Y. J.; Zhang, H.; Huang, Y.; Duan, X. F. *Nano Lett.* **2009**, *9*, 4539–4543.
(41) Zeng, Y. H.; Yang, D. R.; Ma, X. Y.; Zeng, Z. D.; Que, D. L.; Gong, L. F.; Tian, D. X.; Li, L. B. *Mater. Sci. Semicond. Proc.* **2008**, *11*, 131–136.
(42) Peng, K. Q.; Wu, Y.; Fang, H.; Zhong, X. Y.; Xu, Y.; Zhu, J. *Angew. Chem., Int. Ed.* **2005**, *44*, 2737–2742.
(43) Peng, K. Q.; Hu, J. J.; Yan, Y. J.; Wu, Y.; Fang, H.; Xu, Y.; Lee, S. T.; Zhu, J. *Adv. Funct. Mater.* **2006**, *16*, 387–394.